

Spin polarizabilities of the nucleon from polarized low-energy Compton scattering

R.P. Hildebrandt^{1,a}, H.W. Griesshammer^{1,2,b}, and T.R. Hemmert^{1,2,c}

¹ Institut für Theoretische Physik (T39), Physik-Department, Technische Universität München, D-85747 Garching, Germany

² ECT*, Villa Tambosi, I-38050 Villazzano (Trento), Italy

Received: 19 August 2003 / Revised version: 30 October 2003 /

Published online: 27 April 2004 – © Società Italiana di Fisica / Springer-Verlag 2004

Communicated by U.-G. Meißner

Abstract. As a guideline for forthcoming experiments, we present predictions from Chiral Effective Field Theory for polarized cross-sections in low-energy Compton scattering for photon energies below 170 MeV, both on the proton and on the neutron. Special interest is put on the role of the nucleon spin polarizabilities which can be examined especially well in polarized Compton scattering. We present a model-independent way to extract their energy dependence and static values from experiment, interpreting our findings also in terms of the low-energy effective degrees of freedom inside the nucleon: The polarizabilities are dominated by chiral dynamics from the pion cloud, except for resonant multipoles, where contributions of the $\Delta(1232)$ -resonance turn out to be crucial. We therefore include it as an explicit degree of freedom. We also identify some experimental settings which are particularly sensitive to the spin polarizabilities.

PACS. 13.40.-f Electromagnetic processes and properties – 13.60.Fz Elastic and Compton scattering – 14.20.Dh Protons and neutrons

1 Introduction

Over the past few decades, real Compton scattering off the proton was established as an excellent tool to study the polarizabilities of the nucleon —theoretically as well as experimentally. A good overview over the various experiments is given in [1]; for an overlook of the theoretical studies cf. [2, 3] and references therein. As is well known, polarizabilities are a measure for the stiffness of the nucleon in an external electric or magnetic field, caused by the displacement of the charged constituents of the nucleon, induced by the photon field. While the static values $\bar{\alpha}_E, \bar{\beta}_M$ of the two lowest (dipole) spin-independent polarizabilities are well understood, there are only few experiments which are able to extract the *spin polarizabilities* of the nucleon. These quantities have no simple classical analogon, as they parameterize the stiffness of the nucleon spin against electromagnetically induced deformations relative to the axis defined by the nucleon spin. While there are four dipole spin polarizabilities for each nucleon [4], the only two quantities measured so far are the static forward and backward spin polarizabilities γ_0 and γ_π of the proton. γ_0 was extracted from the GDH experiment at

MAMI, using a Dispersion Relation (DR) analysis [1, 5]:

$$\gamma_0 = (-1.01 \pm 0.13) \cdot 10^{-4} \text{ fm}^4. \quad (1.1)$$

A first attempt to determine γ_π from experiment by the LEGS group [6] quotes

$$\gamma_\pi = (-27.1 \pm 3.6) \cdot 10^{-4} \text{ fm}^4, \quad (1.2)$$

which is considerably lower than what one expected from DR analysis and Chiral Effective Field Theory (χ EFT). An extraction from recent MAMI data, obtained at low energies [7] and in the region of the Δ -resonance [8–10], yields values which differ strongly (on a level of about 30%) from the LEGS value:

$$\begin{aligned} \gamma_\pi &= (-36.1 \pm 2.2) \cdot 10^{-4} \text{ fm}^4 \quad [7], \\ \gamma_\pi &= (-37.9 \pm 3.6) \cdot 10^{-4} \text{ fm}^4 \quad [8]. \end{aligned} \quad (1.3)$$

These new results agree very well with the theoretical prediction from χ EFT,

$$\gamma_\pi = -36.7 \cdot 10^{-4} \text{ fm}^4 \quad [11], \quad (1.4)$$

whereas calculations based on χ EFT are at present not able to reproduce the MAMI value for γ_0 , eq. (1.1)¹. For

^a e-mail: rhildebr@ph.tum.de

^b Permanent address: 1; e-mail: hgrie@ph.tum.de

^c Permanent address: 1; e-mail: themmert@ph.tum.de

¹ In the forward direction, a strong cancellation between two large spin polarizabilities makes accurate predictions for γ_0 rather difficult [3].

further details concerning experiments and their results see, *e.g.*, [1].

The goal of this work is to motivate further investigations of the spin polarizabilities, where there are still so many question marks left. Especially, we advocate double-polarized experiments as a tool to disentangle the four leading spin polarizabilities, and not only the two static linear combinations given above.

Recently, it was demonstrated in [12] that nucleon polarizabilities can be connected to Compton multipoles and therefore also acquire a dependence on the energy ω of the real, incoming photon. These dispersion effects are well known in solid state physics. In hadron structure physics different internal nucleonic degrees of freedom, low-lying nuclear resonances like the $\Delta(1232)$, the charged meson cloud around the nucleon etc., will react quite differently to real-photon fields of non-zero frequency. Therefore, these *dynamical polarizabilities* contain detailed information about dispersive effects, caused by internal relaxation effects, baryonic resonances and mesonic production thresholds, see [12, 13] for details. As they stem from a multipole analysis of the scattering amplitude, dynamical polarizabilities contain all hadron structure information, but in a more readily accessible form. In the limit of zero photon energy, they reduce to the static polarizabilities mentioned above.

In principle, the dynamical polarizabilities are experimentally accessible by fits to Compton scattering cross-sections. The main problem seems to be that the multipole expansion allows for an *a priori* infinite number of fit functions: The real photons can undergo transitions $Tl \rightarrow T'l'$, where $T/T' = E$ or M labels the coupling of the incoming/outgoing photon as electric or magnetic, and l , ($l' = l \pm \{0; 1\}$) is the angular momentum of the incident (outgoing) photon. Thus, there are six, ω -dependent dipole polarizabilities, namely the two spin-independent ones $\alpha_{E1}(\omega)$ and $\beta_{M1}(\omega)$ for electric and magnetic dipole transitions which do not couple to the nucleon spin. In the spin sector there are the two diagonal polarizabilities $\gamma_{E1E1}(\omega)$ and $\gamma_{M1M1}(\omega)$ and the two off-diagonal spin polarizabilities $\gamma_{E1M2}(\omega)$ and $\gamma_{M1E2}(\omega)$. In addition, there are higher ones like quadrupole and octupole polarizabilities. In [13], however, it was shown that one can describe unpolarized low-energy Compton scattering off the proton very well by keeping only the $l = 1$ (dipole) contributions of the Compton multipoles. This leaves us with six unknown functions of the photon energy that can be expressed as the six dynamical dipole polarizabilities.

Obviously, further experiments are needed to determine these six functions, as there is, *e.g.*, only a minor dependence on the spin polarizabilities visible in spin-averaged cross-sections below the pion production threshold (see sect. 5). Polarized Compton scattering experiments provide a new avenue for the determination of the six dipole polarizabilities. In the seminal paper [14] on polarized Compton scattering off a nucleon, an exhaustive list of interesting observables and asymmetries was defined which only now start to become accessible in this new frontier of low-energy electromagnetic scattering experiments.

Guided by ongoing experimental feasibility studies at the HI γ S lab of TUNL [15], we chose a subset of four asymmetries describing the interaction of circularly polarized photons with polarized protons and neutrons, where the polarization in the final states is not detected. We cover the low-energy range, up to photon energies of ~ 170 MeV, just above the one-pion production threshold. Like in [14], we focus on asymmetries, dividing the difference of two polarized cross-sections by their sum, as they are less sensitive to experimental errors than differences. Further investigations involving linearly polarized photon beams are under study [16]. We present predictions in the framework of Chiral Effective Field Theory with explicit Δ degrees of freedom. Previously, a calculation of two of the asymmetries for polarized Compton scattering off the proton was presented to leading-one-loop order in a χ EFT with only nucleon and pion degrees of freedom in [17]. In our analysis (sects. 6 and 7) we show a comparison between the two chiral frameworks for all asymmetries we consider, so that Δ physics is easily identifiable. Since we investigate the possibility of determining spin polarizabilities from experiment, we put special emphasis on the role of the spin and quadrupole ($l = 2$) polarizabilities of the nucleon. The latter ones will —as in [13] for the spin-averaged case— turn out to be negligibly small, leaving only the six dynamical dipole polarizabilities as unknown structure parameters to be determined from data. As a starting point, one might consequently accept the theoretical findings for the spin-independent dipole polarizabilities $\alpha_{E1}(\omega)$, $\beta_{M1}(\omega)$, for which both χ EFT and Dispersion analysis are in good agreement [13]. One would then attempt to extract the four dynamical $l = 1$ spin polarizabilities directly from experiment, as will be described in sect. 4.

In [14], the authors also investigated the energy dependence of various asymmetries both in a low-energy expansion in terms of nucleon polarizabilities as well as in a full calculation in Dispersion Theory. The low-energy expansion included the static values of the six dipole polarizabilities, the two static spin-independent quadrupole polarizabilities $\bar{\alpha}_{E2}$, $\bar{\beta}_{M2}$, and the leading dispersion corrections to $\bar{\alpha}_{E1}$ and $\bar{\beta}_{M1}$. Such a Taylor expansion of the polarizabilities is bound to break down as cusps or resonances are approached, the lowest of which being the one-pion production threshold and the Δ -resonance. We will indeed find strong signals from the spin polarizabilities as the energy is increased. In contradistinction to [14], our calculation is based on *dynamical*, *i.e.* energy-dependent polarizabilities [12]. For photon energies above the pion production threshold, we expect our predictions to be correct only qualitatively, since the imaginary parts of our dynamical polarizabilities only correspond to tree-level accuracy and the width of the $\Delta(1232)$ -resonance is treated as a small perturbation; for details, see [13]. Whereas the unpolarized cross-sections were found to be well described up to 170 MeV within our theoretical framework [13], we have to caution the reader that this does not have to be the case for the asymmetries presented here, as these are much more sensitive to fine details.

The two spin configurations we investigate are described in sect. 3, after a short repetition of the theoretical framework (sect. 2). In sect. 4, we propose a procedure to determine spin polarizabilities from experiment, before we have another look at spin-averaged cross-sections in sect. 5. The results for the proton asymmetries are presented and interpreted in sect. 6, the ones for the neutron in sect. 7. Conclusions and an appendix on the two dominating Compton amplitudes complete the presentation.

2 Theoretical framework

We calculate in the framework of Chiral Effective Field Theory with and without explicit $\Delta(1232)$ degrees of freedom. Details concerning the former, Heavy Baryon Chiral Perturbation Theory (HB χ PT), which contains only pions and nucleons as explicit degrees of freedom, can be found, *e.g.*, in [17]. The formalism of the latter, called ‘‘Small Scale Expansion’’ (SSE) —an effective chiral field theory describing explicit pion, nucleon and $\Delta(1232)$ degrees of freedom— is discussed in [18]. This work is based on the calculation of dynamical nucleon polarizabilities and spin-averaged Compton cross-sections of the proton in [13] to which we refer the interested reader for details of our notation.

Real Compton scattering can be formulated in terms of six amplitudes² A_1 – A_6 . The T -matrix reads

$$\begin{aligned} T(\omega, z) = & A_1(\omega, z) \vec{\epsilon}'^* \cdot \vec{\epsilon} + A_2(\omega, z) \vec{\epsilon}'^* \cdot \hat{k} \vec{\epsilon} \cdot \hat{k}' \\ & + i A_3(\omega, z) \vec{\sigma} \cdot (\vec{\epsilon}'^* \times \vec{\epsilon}) + i A_4(\omega, z) \vec{\sigma} \cdot \left(\hat{k}' \times \hat{k} \right) \vec{\epsilon}'^* \cdot \vec{\epsilon} \\ & + i A_5(\omega, z) \vec{\sigma} \cdot \left[\left(\vec{\epsilon}'^* \times \hat{k} \right) \vec{\epsilon} \cdot \hat{k}' - \left(\vec{\epsilon} \times \hat{k}' \right) \vec{\epsilon}'^* \cdot \hat{k} \right] \\ & + i A_6(\omega, z) \vec{\sigma} \cdot \left[\left(\vec{\epsilon}'^* \times \hat{k}' \right) \vec{\epsilon} \cdot \hat{k} - \left(\vec{\epsilon} \times \hat{k} \right) \vec{\epsilon}'^* \cdot \hat{k}' \right] \end{aligned} \quad (2.1)$$

with \hat{k} (\hat{k}') the unit vector in the momentum direction of the incoming (outgoing) photon with polarization $\vec{\epsilon}$ ($\vec{\epsilon}'^*$). We separate these amplitudes into pole (A_i^{pole}) and non-pole (\bar{A}_i) parts.

The non-pole amplitudes are also referred to as the structure part of the amplitudes. The question whether a contribution belongs to the structure part cannot be answered uniquely. In our definition, only those terms which have a pole either in the s -, u - or t -channel are treated as non-structure. If we were only concerned with the full calculation of Compton scattering cross-sections, this separation clearly would be irrelevant because both the structure-dependent as well as the structure-independent part contribute. Here, however, we investigate the role of the internal nucleonic degrees of freedom on the spin and quadrupole polarizabilities in Compton scattering. Therefore, we need to be able to turn off and on the different

nucleon polarizabilities, which are contained only in the structure part of the amplitudes.

Expressing the $l = 1$ multipole expansion for nucleon Compton scattering in terms of dynamical dipole polarizabilities, one obtains

$$\begin{aligned} \bar{A}_1(\omega, z) &= \frac{4\pi W}{M} [\alpha_{E1}(\omega) + z \beta_{M1}(\omega)] \omega^2 + \mathcal{O}(l = 2), \\ \bar{A}_2(\omega, z) &= -\frac{4\pi W}{M} \beta_{M1}(\omega) \omega^2 + \mathcal{O}(l = 2), \\ \bar{A}_3(\omega, z) &= -\frac{4\pi W}{M} \left[\gamma_{E1E1}(\omega) + z \gamma_{M1M1}(\omega) \right. \\ &\quad \left. + \gamma_{E1M2}(\omega) + z \gamma_{M1E2}(\omega) \right] \omega^3 + \mathcal{O}(l = 2), \\ \bar{A}_4(\omega, z) &= \frac{4\pi W}{M} \left[-\gamma_{M1M1}(\omega) \right. \\ &\quad \left. + \gamma_{M1E2}(\omega) \right] \omega^3 + \mathcal{O}(l = 2), \\ \bar{A}_5(\omega, z) &= \frac{4\pi W}{M} \gamma_{M1M1}(\omega) \omega^3 + \mathcal{O}(l = 2), \\ \bar{A}_6(\omega, z) &= \frac{4\pi W}{M} \gamma_{E1M2}(\omega) \omega^3 + \mathcal{O}(l = 2). \end{aligned} \quad (2.2)$$

We choose to work in the centre-of-mass frame. Thus, ω denotes the cm energy of the photon, M the isoscalar nucleon mass, $W = \sqrt{s}$ the total cm energy, and θ the cm scattering angle with $z = \cos \theta$.

The structure amplitudes \bar{A}_3 – \bar{A}_6 contain only spin polarizabilities, \bar{A}_1 – \bar{A}_2 only spin-independent ones. The spin polarizabilities γ_0 (γ_π) mentioned in the introduction are the leading coefficients of \bar{A}_3 for $\theta = 0^\circ$ ($\theta = 180^\circ$) at zero energy:

$$\begin{aligned} \gamma_0 &= -(\bar{\gamma}_{E1E1} + \bar{\gamma}_{M1M1} + \bar{\gamma}_{E1M2} + \bar{\gamma}_{M1E2}), \\ \gamma_\pi &= -\bar{\gamma}_{E1E1} + \bar{\gamma}_{M1M1} - \bar{\gamma}_{E1M2} + \bar{\gamma}_{M1E2} \end{aligned}$$

and thus do not suffice to determine the four leading spin polarizabilities completely. Here, $\bar{\gamma}_i$ denotes the static limit $\bar{\gamma}_i = \gamma_i(\omega = 0)$. A precise definition of polarizabilities via the multipole expansion of the amplitudes is given in [13].

In the following, we list all the diagrams contributing in our leading-one-loop order ($\mathcal{O}(\epsilon^3)$) calculation in the Small Scale Expansion, which contains the leading chiral dynamics of the pion cloud and the dominant Δ physics with its pionic cloud. ϵ is the expansion parameter of SSE and denotes either a small momentum, the pion mass or the mass difference between nucleon and $\Delta(1232)$. A diagram at a certain order in p containing pions in the theory without explicit Δ degrees of freedom, HB χ PT, contributes at the same order ϵ in SSE.

In fig. 1, we show the four HB χ PT non-structure (pole) diagrams which contribute to an $\mathcal{O}(p^3)$ (and therefore also to an $\mathcal{O}(\epsilon^3)$) calculation: the pole diagrams (a,b), the Thomson term (c) and the ‘‘pion pole’’ (d). The pole parts are thus given by the amplitudes of Compton scattering off a point-like nucleon with an anomalous magnetic moment, in addition to the π^0 -pole contribution in the t -channel. In the literature, the latter contribution is sometimes classified as a structure part.

² These amplitudes are different from the amplitudes A_i in [14], as we use a different basis.

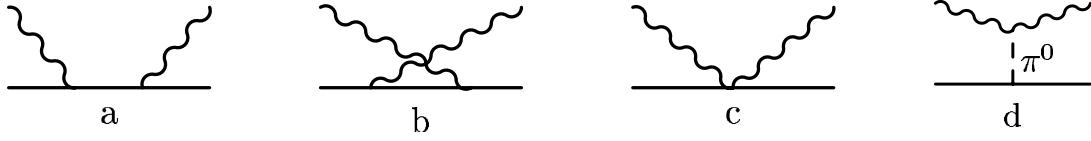


Fig. 1. The diagrams identified as pole contributions at leading-one-loop order in HB χ PT.

To $\mathcal{O}(\epsilon^3)$, one obtains for the non-structure amplitudes (with the charge $Q = 1$ for a proton, $Q = 0$ for a neutron target)

$$\begin{aligned}
 A_1^{\text{pole}}(\omega, \theta) &= -\frac{Q e^2}{M} + \mathcal{O}(\epsilon^4), \\
 A_2^{\text{pole}}(\omega, \theta) &= \frac{Q^2 e^2 \omega}{M^2} + \mathcal{O}(\epsilon^4), \\
 A_3^{\text{pole}}(\omega, \theta) &= \frac{e^2 \omega (Q(1+2\kappa) - (Q+\kappa)^2 \cos\theta)}{2M^2} \\
 &\quad - (2Q-1) \frac{e^2 g_A}{4\pi^2 f_\pi^2} \frac{\omega^3 (1-\cos\theta)}{m_{\pi^0}^2 + 2\omega^2 (1-\cos\theta)} + \mathcal{O}(\epsilon^4), \\
 A_4^{\text{pole}}(\omega, \theta) &= -\frac{e^2 \omega (Q+\kappa)^2}{2M^2} + \mathcal{O}(\epsilon^4), \\
 A_5^{\text{pole}}(\omega, \theta) &= \frac{e^2 \omega (Q+\kappa)^2}{2M^2} \\
 &\quad - (2Q-1) \frac{e^2 g_A}{8\pi^2 f_\pi^2} \frac{\omega^3}{m_{\pi^0}^2 + 2\omega^2 (1-\cos\theta)} + \mathcal{O}(\epsilon^4), \\
 A_6^{\text{pole}}(\omega, \theta) &= -\frac{e^2 \omega Q (Q+\kappa)}{2M^2} \\
 &\quad + (2Q-1) \frac{e^2 g_A}{8\pi^2 f_\pi^2} \frac{\omega^3}{m_{\pi^0}^2 + 2\omega^2 (1-\cos\theta)} + \mathcal{O}(\epsilon^4).
 \end{aligned} \tag{2.3}$$

κ is the anomalous magnetic moment of the proton or the neutron, respectively, e the proton's electric charge. m_{π^0} is the mass of the neutral pion, f_π the pion decay constant. The terms containing the axial coupling constant g_A are the contributions of the pion pole. The numerical values we use are listed in table 1 in [13] and correspond to [19].

Besides the pole terms, our calculation includes all leading-one-loop order HB χ PT diagrams [20]. To this order, they contain only pion cloud effects around the nucleon. In SSE, the diagrams at order ϵ^3 in addition to the HB χ PT ones are the $\Delta\pi$ continuum and Δ pole diagrams [11, 21]. As all these diagrams have already been sketched in [13], we refrain from showing them once again and refer the interested reader to figs. 2-4 in [13]. We emphasize that there is no difference in the structure part of the amplitudes between proton and neutron up to $\mathcal{O}(\epsilon^3)$. Therefore, our non-pole amplitudes describe an isoscalar nucleon and the only difference between the two nucleons comes in via the pole amplitudes eq. (2.3). As the analytic expressions for the structure amplitudes are rather lengthy, we refer the reader to [13] for a complete listing.

As discussed in [13] we require two additional operators, which are energy-independent and contribute only to

the spin-independent dipole polarizabilities. These terms are formally $\mathcal{O}(\epsilon^4)$, but turn out to be anomalously large [13] and therefore have to be taken into account already at leading-one-loop order. Their numerical values are determined by a fit to unpolarized Compton scattering data. The static, spin-independent dipole polarizabilities $\bar{\alpha}_E$ and $\bar{\beta}_M$ thus obtained are in excellent agreement to and of comparable uncertainty as the results from alternative extractions, see [13] for details.

We now turn to the formalism of Compton cross-sections.

3 Cross-sections and asymmetries —formalism

The well-known formula for Compton cross-sections in the cm frame is

$$\frac{d\sigma}{d\Omega} \Big|_{\text{cm}} = \left(\frac{M}{4\pi W} \right)^2 |T|^2. \tag{3.1}$$

In [13], we showed results for unpolarized proton cross-sections, which are derived by averaging over the initial and summing over the final spin states. Now, we concentrate on spin-polarized cross-sections for proton and neutron, albeit we will return briefly to spin-averaged ones in sect. 5.

Triggered by a forthcoming proposal on polarized Compton scattering off ^3He at the HI γ S lab of TUNL [15], we choose the incoming photon to be right-circularly polarized,

$$\vec{\epsilon} = \frac{1}{\sqrt{2}} \begin{pmatrix} 1 \\ i \\ 0 \end{pmatrix}$$

and moving along the positive z -direction, while the final polarization and nucleon spin remain undetected. The two nucleon spin configurations we investigate are

- 1) the difference between the target nucleon spin pointing parallel or antiparallel to the incident-photon momentum

$$\frac{d\sigma_{\uparrow\uparrow}}{d\Omega_{\text{cm}}} - \frac{d\sigma_{\uparrow\downarrow}}{d\Omega_{\text{cm}}};$$

- 2) the difference between the target nucleon spin aligned in the positive or negative x -direction:

$$\frac{d\sigma_{\uparrow\rightarrow}}{d\Omega_{\text{cm}}} - \frac{d\sigma_{\uparrow\leftarrow}}{d\Omega_{\text{cm}}}.$$

The first arrow in our notation denotes the direction of the incoming, right-circularly polarized photon, the second one the direction of the nucleon spin.

The corresponding formulae for $|T|^2$ can already be found in [17], albeit there they are given only for real amplitudes A_1 – A_6 . As is well known, these amplitudes become complex for a photon energy above the pion production threshold ω_π . Including the imaginary part of the amplitudes, the formulae read

$$\begin{aligned} \frac{1}{2} (|T|_{\uparrow\uparrow}^2 - |T|_{\uparrow\downarrow}^2) &= -\text{Re}[A_1 A_3^*] (1 + \cos^2 \theta) \\ &- \left[|A_3|^2 + 2 |A_6|^2 + 2 |A_5|^2 \cos^2 \theta + \text{Re}[A_6 (A_1^* + 3 A_3^*)] \right. \\ &+ \left. \left(\text{Re}[A_3 (3 A_5^* + A_4^* - A_2^*)] + \text{Re}[A_5 (4 A_6^* - A_1^*)] \right) \cos \theta \right. \\ &\left. + \text{Re}[A_5 (A_2^* - A_4^*)] \sin^2 \theta \right] \sin^2 \theta \end{aligned} \quad (3.2)$$

and

$$\begin{aligned} \frac{1}{2} (|T|_{\uparrow\rightarrow}^2 - |T|_{\uparrow\leftarrow}^2) &= \\ &\left[\text{Im}[A_1 (A_3^* + 2 A_6^* + 2 A_5^* \cos \theta)] \cos \theta \right. \\ &+ \text{Im}[A_1 A_4^*] (1 + \cos^2 \theta) - \text{Im}[A_2 (A_3^* + 2 A_6^*)] \sin^2 \theta \\ &\left. - \text{Im}[A_2 (A_4^* + 2 A_5^*)] \cos \theta \sin^2 \theta \right] \sin \theta \sin \phi \\ &+ \left[\text{Re}[A_3 (A_3^* - A_1^* + 2 A_6^*)] \cos \theta \right. \\ &+ \text{Re}[A_3 A_5^*] (3 \cos^2 \theta - 1) \\ &+ \left(\text{Re}[A_1 A_5^*] + \text{Re}[A_2 A_3^*] \right. \\ &+ \left. \text{Re}[A_6 (A_2^* + A_4^* - 2 A_5^*)] \right) \sin^2 \theta \\ &+ \text{Re}[A_3 A_4^*] (\cos^2 \theta + 1) \\ &\left. + \text{Re}[A_5 (A_2^* - A_4^* - 2 A_5^*)] \cos \theta \sin^2 \theta \right] \sin \theta \cos \phi. \end{aligned} \quad (3.3)$$

Here, ϕ is the angle between the reaction plane and the plane spanned by the momentum of the incoming photon and the target nucleon spin. Obviously, the difference eq. (3.3) takes on the largest values—at least below the pion production threshold—for $\phi = 0$. Therefore, we choose the nucleon spin in the reaction plane, which simplifies eq. (3.3) considerably. Using left- instead of right-circularly polarized photons changes only the overall sign in eqs. (3.2) and (3.3).

For comparison, we show once again $|T|^2$ for the spin-averaged cross-section [17], which can be derived by taking the sum instead of the difference in eq. (3.2) (or as well in

eq. (3.3)):

$$\begin{aligned} \frac{1}{2} (|T|_{\uparrow\uparrow}^2 + |T|_{\uparrow\downarrow}^2) &= \frac{1}{2} |A_1|^2 (1 + \cos^2 \theta) \\ &+ \frac{1}{2} |A_3|^2 (3 - \cos^2 \theta) + \left[\frac{1}{2} |A_4|^2 (1 + \cos^2 \theta) \right. \\ &+ \frac{1}{2} |A_2|^2 \sin^2 \theta + |A_5|^2 (1 + 2 \cos^2 \theta) \\ &+ 3 |A_6|^2 + 4 \text{Re}[A_3 A_6^*] + 2 \text{Re}[A_4 A_5^*] \cos^2 \theta \\ &+ \left(-\text{Re}[A_1 A_2^*] + \text{Re}[A_3 (A_4^* + 2 A_5^*)] \right. \\ &\left. + 2 \text{Re}[A_6 (A_4^* + 3 A_5^*)] \right) \cos \theta \left. \right] \sin^2 \theta. \end{aligned} \quad (3.4)$$

The asymmetries we consider³ are

$$\Sigma_z = \frac{|T|_{\uparrow\uparrow}^2 - |T|_{\uparrow\downarrow}^2}{|T|_{\uparrow\uparrow}^2 + |T|_{\uparrow\downarrow}^2}, \quad (3.5)$$

$$\Sigma_x = \frac{|T|_{\uparrow\rightarrow}^2 - |T|_{\uparrow\leftarrow}^2}{|T|_{\uparrow\rightarrow}^2 + |T|_{\uparrow\leftarrow}^2}. \quad (3.6)$$

Σ is a frame-independent quantity, as the frame-dependent flux factor cancels in the ratio between difference and sum of the cross-section, while $|T|^2$ can be written in terms of the frame-independent Mandelstam variables.

From the experimentalist's point of view, it is more convenient to measure the *asymmetry*—*i.e.* the difference divided by the sum—instead of the differences eqs. (3.2) and (3.3), as the former is more tolerant to systematic errors in experiments. Nevertheless, we have to caution the reader that division by a small quantity, say a small spin-averaged cross-section, may enhance theoretical uncertainties. Sensitivity to the nucleon structure, *e.g.* the spin polarizabilities, may be lost by dividing the difference by the sum. Whenever this happens in sects. 6 and 7, we will give hints in the text, but we refrain from showing our results for the differences eqs. (3.2), (3.3) for reasons of compactification, as there is no hope to compare with experimental data for absolute values of polarized Compton cross-sections within the next few years.

4 Extracting spin polarizabilities from experiment

A first step in determining dynamical spin polarizabilities from experiment might be to accept our findings for the spin-independent dipole polarizabilities $\alpha_{E1}(\omega)$ and $\beta_{M1}(\omega)$, which show very good agreement with Dispersion Relation analysis up to about 170 MeV [13]. Truncating at $l = 1$, this leaves no unknowns in A_1 and A_2 . As higher polarizabilities are negligible, the spin-dependent dipole polarizabilities could then be fitted to data sets which combine polarized and spin-averaged experimental

³ Σ_z corresponds to Σ_{2z} in the notation of [14], Σ_x to Σ_{2x} .

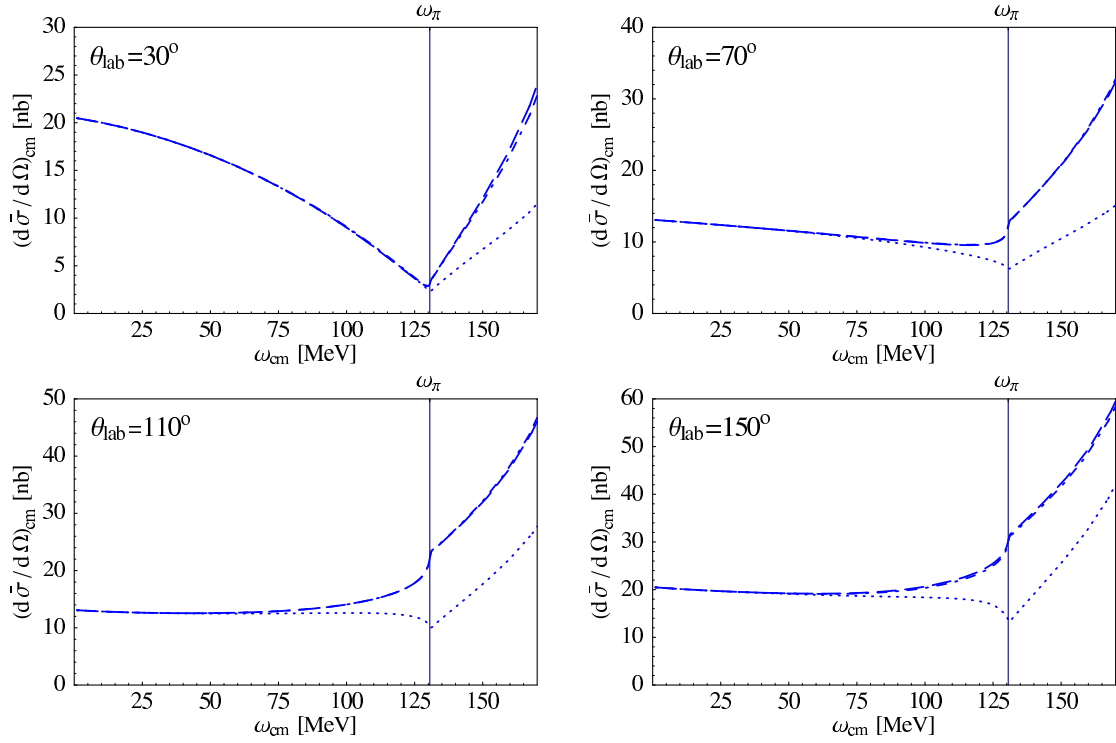


Fig. 2. Complete $\mathcal{O}(\epsilon^3)$ SSE predictions (dashed line) for the spin-averaged proton cross-section; dotted line: spin polarizabilities not included; dot-dashed line: quadrupole polarizabilities not included. ω_π denotes the pion production threshold.

results, taken at a fixed energy and varying the scattering angle. As starting values for the fit, one might use our χ EFT results [13], as indicated in eq. (4.1), where we show the spin structure amplitudes up to $l = 1$ with the polarizabilities $\gamma_i(\omega)$ replaced by $\gamma_i(\omega) + \delta_i$, introducing the fit parameters δ_i . Small fit parameters mean correct prediction of the dynamical spin dipole polarizabilities within the Small Scale Expansion.

$$\begin{aligned}
 \bar{A}_3^{\text{fit}}(\omega, z) &= -\frac{4\pi W}{M} \left[(\gamma_{E1E1}(\omega) + \delta_{E1E1}) \right. \\
 &\quad + z(\gamma_{M1M1}(\omega) + \delta_{M1M1}) + (\gamma_{E1M2}(\omega) + \delta_{E1M2}) \\
 &\quad \left. + z(\gamma_{M1E2}(\omega) + \delta_{M1E2}) \right] \omega^3, \\
 \bar{A}_4^{\text{fit}}(\omega, z) &= \frac{4\pi W}{M} \left[-(\gamma_{M1M1}(\omega) + \delta_{M1M1}) \right. \\
 &\quad \left. + (\gamma_{M1E2}(\omega) + \delta_{M1E2}) \right] \omega^3, \\
 \bar{A}_5^{\text{fit}}(\omega, z) &= \frac{4\pi W}{M} (\gamma_{M1M1}(\omega) + \delta_{M1M1}) \omega^3, \\
 \bar{A}_6^{\text{fit}}(\omega, z) &= \frac{4\pi W}{M} (\gamma_{E1M2}(\omega) + \delta_{E1M2}) \omega^3. \quad (4.1)
 \end{aligned}$$

Thus, one obtains the spin dipole polarizabilities at a definite energy. Repeating this procedure for various energies gives the energy dependence, *i.e.* the dynamics of the $l = 1$ spin polarizabilities. Therefore, the amplitudes eq. (4.1) provide one possible way to extract dynamical spin polarizabilities directly from the asymmetry observables of the previous section, using χ EFT. Note that the δ_i may show a weak energy dependence. At first trial, they can be

taken as energy-independent quantities. This corresponds to a free normalization of the spin dipole polarizabilities, assuming the energy dependence derived from χ EFT to be correct. This assumption is well justified, as at low energies only $\Delta(1232)$ and pion degrees of freedom are supposed to give dispersive contributions to the polarizabilities.

5 Spin contributions to spin-averaged cross-sections

Before discussing the asymmetries in detail, we briefly turn to the question of which polarizabilities are seen in unpolarized Compton cross-sections, discussing the $\mathcal{O}(\epsilon^3)$ SSE results partially given already in [13]. As shown in fig. 2, we find a large contribution of the dynamical spin polarizabilities to spin-averaged Compton cross-sections on the proton above $\omega \sim 100$ MeV. We also show our so far unpublished results for the neutron (fig. 3), exhibiting a huge sensitivity to the spin polarizabilities in the backward direction. This can be well understood, as the right-hand side of eq. (3.4) simplifies to $|A_1|^2 + |A_3|^2$ for $\theta = 0^\circ$ and $\theta = 180^\circ$. In the forward direction, the spin-independent amplitude $|A_1|^2$ dominates, while in the backward direction the spin-dependent amplitude $|A_3|^2$ is dominant, as can be seen in appendix A.

We note also again that any effects of quadrupole polarizabilities are invisible at the level of the unpolarized cross-sections, as has already been found in [13] for the proton. It suffices therefore to terminate the multipole

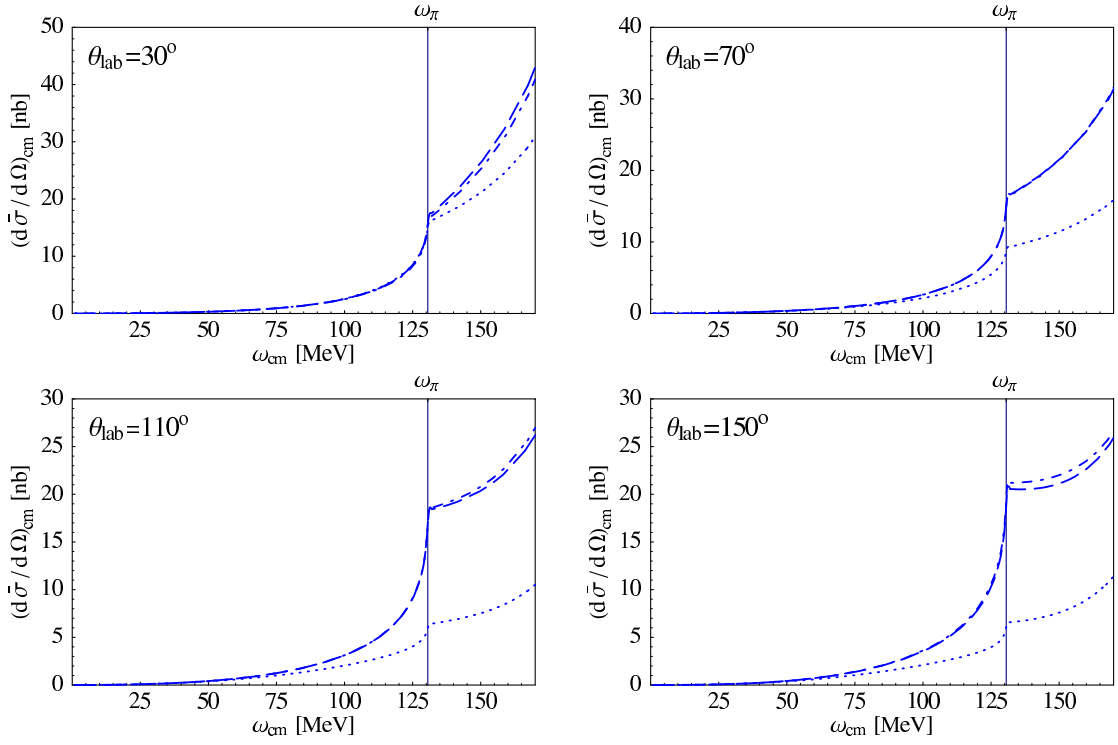


Fig. 3. Spin-averaged neutron cross-section; for notations see fig. 2.

expansion eq. (2.2) at the dipole level, which leaves the six dipole polarizabilities as parameters.

While effects from the spin polarizabilities are non-negligible in unpolarized experiments, to extract all four of them from such data is clearly illusory. Thus, double-polarized experiments as discussed in the rest of this article are necessary additional ingredients in a combined multipole analysis.

6 Proton asymmetries

We therefore turn now to the results for the asymmetries of the proton. Analogously to the previous section, we confirm for each observable that the quadrupole polarizabilities are negligible. Thus, the multipole expansion of the amplitude can always be truncated at the dipole level, leaving at most six parameters. However, it will turn out that not all asymmetries are equally sensitive to the spin polarizabilities. As expected, most asymmetries are indeed governed by the pole part of the amplitudes.

In order to determine which asymmetries are most sensitive to the structure parts of the Compton amplitudes, and which of the internal low-energy degrees of freedom in the nucleon dominate the structure-dependent part of the cross-section, we will first compare three scenarios for each asymmetry: i) the result when only the pole terms of the amplitudes are kept; ii) the same when the effects from the pion cloud around the nucleon are added, as described by the leading-one-loop order HB χ PT result; and finally iii) a leading-one-loop order calculation in SSE, including also the Δ as dynamical degree of freedom.

An ideal asymmetry should thus fulfill three criteria: It should be large to give a good experimental signal, it should show sensitivity to the structure amplitudes, and it should allow a differentiation between the pion cloud and Δ -resonance contributions in resonant channels, revealing as much as possible about the role of at least these low-energy degrees of freedom in the nucleon. In sect. 7, we will repeat this presentation for the neutron asymmetries. To simplify the connection to experiment, we give the scattering angle in the following plots in the lab frame.

Similar plots for the nucleon asymmetries have already been shown in [14], using Dispersion Theory techniques. Direct comparison to those plots is however not possible because of a different choice of angles—the authors of [14] concentrated on the extreme angles 0° , 90° , 180° , whereas we cover the whole experimentally accessible angular spectrum. Nevertheless, qualitative agreement between our χ EFT results and [14] can be deduced.

We emphasize also that our predictions are parameter free, as all constants are determined from unpolarized Compton scattering on the proton, [13]. In the following the fit parameters δ_i introduced in eq. (4.1) are all set to zero, as no measured asymmetries exist at this point.

6.1 Nucleon spin parallel photon momentum

6.1.1 Comparison: pole, HB χ PT and SSE calculation of Σ_z^p

As one can see in fig. 4, the proton asymmetry Σ_z^p reaches values of $\mathcal{O}(1)$ and is therefore quite large, although it

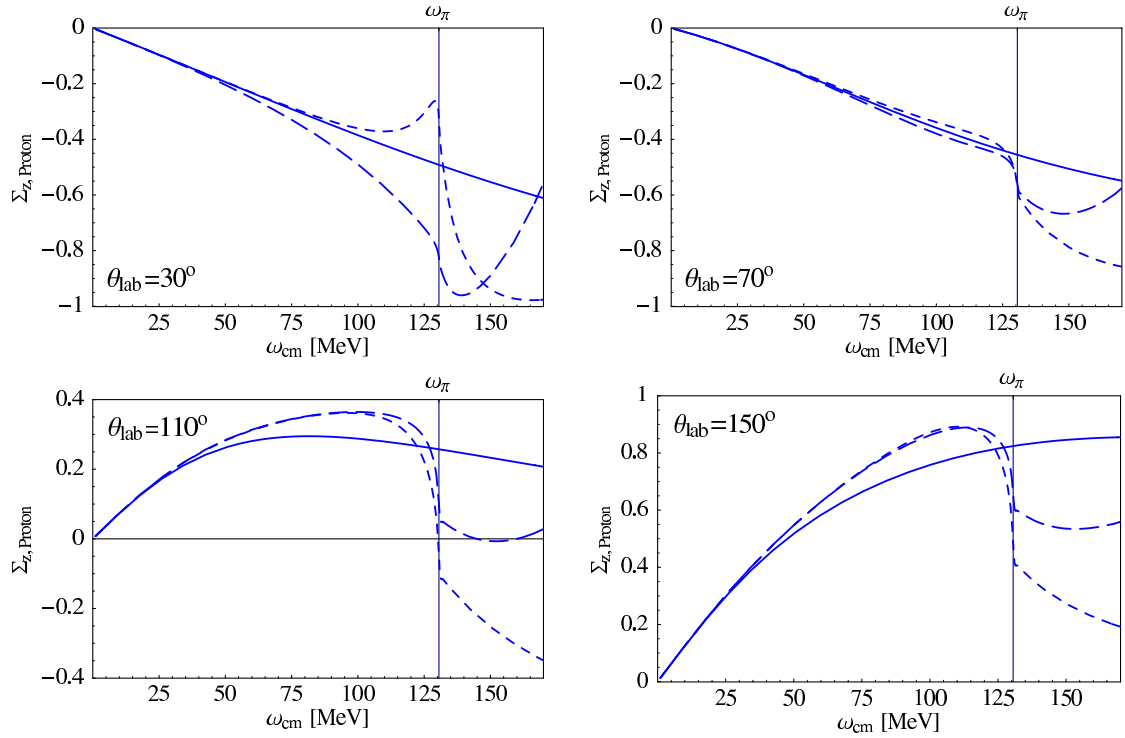


Fig. 4. $\mathcal{O}(p^3)$ HB χ PT (short-dashed line) and $\mathcal{O}(\epsilon^3)$ SSE predictions (long-dashed line) for the proton asymmetry Σ_z^p ; the solid line describes the third-order pole contributions. ω_π denotes the pion production threshold.

vanishes for $\omega = 0$, due to the vanishing difference and the finite static spin-averaged cross-section, given by the familiar Thomson limit. This is valid independently of the scattering angle.

Comparing the three curves in fig. 4—third-order pole, $\mathcal{O}(p^3)$ HB χ PT and $\mathcal{O}(\epsilon^3)$ SSE—one recognizes the strong influence of the pole amplitudes, given by eq. (2.3). This is exactly what one expects for the charged proton, and can also be deduced from eqs. (2.2), (2.3), (3.2): The asymmetry starts linearly in ω , while the leading term of the structure part of Σ_z^p is proportional to ω^3 , as there is no term in eq. (3.2) that contains only spin-independent amplitudes. As we are interested in information about the structure of the nucleon, *i.e.* in the deviation of the dashed lines from the solid (pole contributions only) line in fig. 4, and as this deviation is not as strong as later in Σ_x^p and in the neutron asymmetries, Σ_z^p does not seem to be the ideal choice among the considered quantities to examine the nucleon structure.

Concerning the explicit Δ degrees of freedom, we see sizeable contributions only above ω_π . The only exception is noticed in the extreme forward direction, but this is an artifact of the asymmetry, which is extremely sensitive at small angles due to the small spin-averaged cross-section at ω_π (fig. 2), and neither visible in the difference, described by eq. (3.2), nor in the spin-averaged cross-section.

The structure of Σ_z^p varies a lot for the different angles. It is negative in the forward and positive in the backward direction. This can be explained—at least for low energies (≤ 120 MeV)—looking at the amplitudes A_1 and A_3 in

fig. 12 below because for $\theta = 0^\circ$ and $\theta = 180^\circ$ the right-hand side of eq. (3.2) reduces to $-2A_1A_3$. The proton amplitude A_3 starts with a falling slope in the forward and with a rising slope in the backward direction, while A_1 is negative below the pion production threshold for all angles under consideration. The spin-averaged cross-section is positive for all angles and energies by definition.

At $\omega_\pi \approx 131$ MeV in the cm system, the cusp at the pion production threshold is clearly visible for most of the angles. This cusp arises since the amplitudes become complex at the threshold. Polarized cross-sections are much more sensitive to the fine structure of the nucleon than their unpolarized pendants. Therefore, our results might considerably deviate from experiment above threshold, due to sizeable uncertainties in our imaginary parts. Nevertheless, qualitative agreement should be fulfilled, so we use the same plot range as for the unpolarized results in [13], with a maximum photon energy of 170 MeV. In [14], the plots end below threshold since the low-energy expansion of the polarizabilities used in [14] cannot reproduce the non-analyticity of the pion production threshold.

6.1.2 Spin and quadrupole contributions to Σ_z^p

The asymmetry (fig. 5) exhibits only a weak dependence on the spin polarizabilities in the forward direction below ω_π , which is no surprise, as in fig. 12 below there are nearly no structure contributions to A_3^p visible below 100 MeV. The largest sensitivity on the γ_i 's is noted at around 110° , whereas in the extreme backward direction

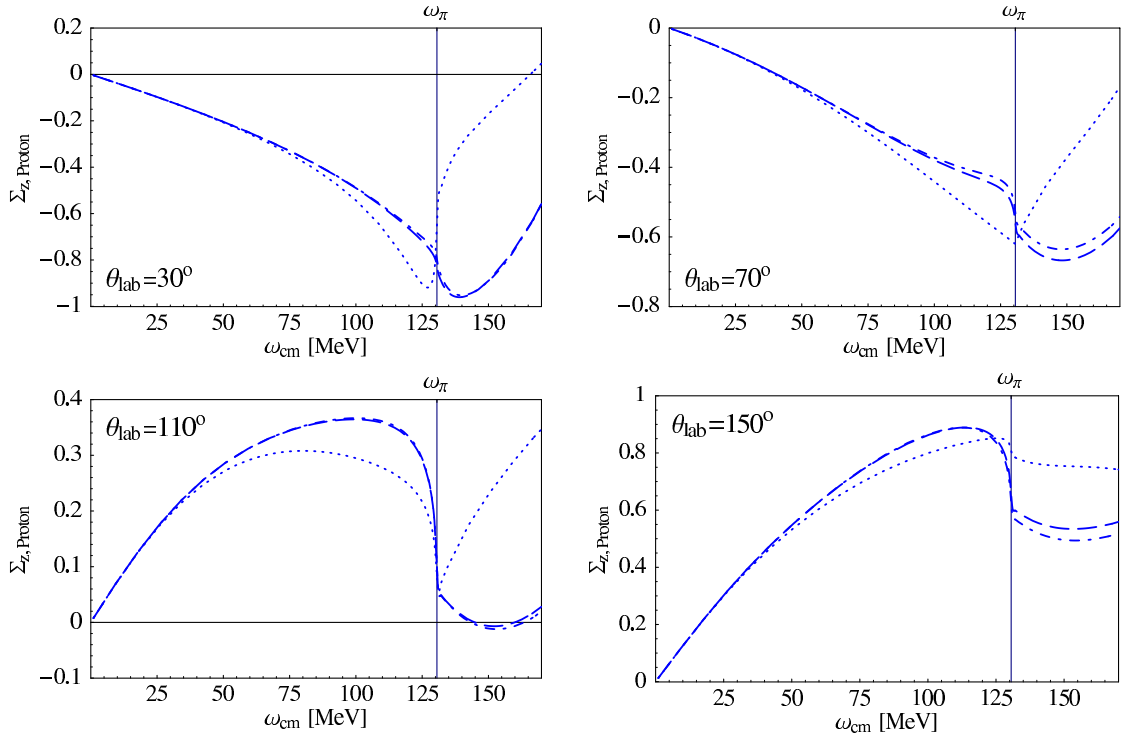


Fig. 5. Proton asymmetry Σ_z^p ; for notations see fig. 2.

the dependence on the spin polarizabilities partly cancels in the division of the difference by the sum.

The sharp rise of the result without spin polarizabilities in fig. 5 above the pion production threshold in the forward direction is due to a sharply rising difference and the small spin-averaged cross-section which enters the denominator presented in fig. 2.

In the literature, *e.g.* in [6], the pion pole (fig. 1d) is often considered as one of the structure diagrams, giving a contribution to the static backward spin polarizability γ_π , which is much larger than all the other contributions. We treat the term as pole, as it contains a pion pole in the t -channel. So the question arises of why we are sensitive to the spin polarizabilities, despite having removed this supposedly dominant part from them. The reason is that the pion pole dominates over the structure part of γ_π only for low energies. The pion pole contribution to $\gamma_\pi(\omega)$ describes a Lorentzian (eq. (2.3)) and becomes smaller than the structure contribution above 100 MeV, as the latter one rises due to the increasing values of $\gamma_{E1E1}(\omega)$ and $\gamma_{M1M1}(\omega)$ [13].

It is crucial to notice that the quadrupole polarizabilities ($l = 2$) play again a negligibly small role, see fig. 5. The most important quadrupole contribution is observed at 70° and 150° , but the relative size is still < 0.1 and therefore presumably within the experimental error bars. As repeatedly stated, that these contributions are small is mandatory if one wants to determine spin polarizabilities via polarized-cross-section data, because only then can the multipole expansion be truncated at $l = 1$ as in eqs. (2.2), (4.1).

6.2 Nucleon spin perpendicular to photon momentum

6.2.1 Comparison: pole, HB χ PT and SSE calculation of Σ_x^p

The asymmetry Σ_x^p in fig. 6 looks quite similar for the different angles: It always starts with a falling slope and exhibits a sharp minimum at the pion cusp, therefore staying negative in a wide energy range. This behaviour is no surprise, as the leading term in eq. (3.3) for the proton for $\theta \approx 0^\circ$, $\theta \approx 180^\circ$, *i.e.* $\sin^2 \theta \approx 0$, is $A_3 (A_3 - A_1) \sin \theta \cos \theta$, which is the only term including A_1 and therefore dominating for low energies, as A_1^p contains the Thomson limit. In both the forward and the backward direction $A_3 - A_1 > 0$, and $A_3 < (>) 0$ for small (large) angles and low energies. The factor $\cos \theta$ gives an additional minus sign in the backward direction.

Even more striking than for Σ_z^p is the weak sensitivity of the asymmetry Σ_x^p to explicit Δ degrees of freedom. Once again, the only exception to this rule is the extreme forward direction because of the small spin-averaged cross-section which enhances the small deviations between the HB χ PT and the SSE calculation of the difference eq. (3.3) and makes Σ_x^p extremely sensitive to errors. Therefore, we consider the forward-angle regime as inconvenient for measuring proton asymmetries. In the other panels of fig. 6 the Δ -dependence cancels in the asymmetry, whereas we found the $\Delta(1232)$ -resonance to give sizeable contributions to both the difference and the sum. This is one example that an asymmetry actually hides interesting physical information.

The dominance of the pole amplitudes is —as in Σ_z^p — clearly visible. The argument is the same as the one given

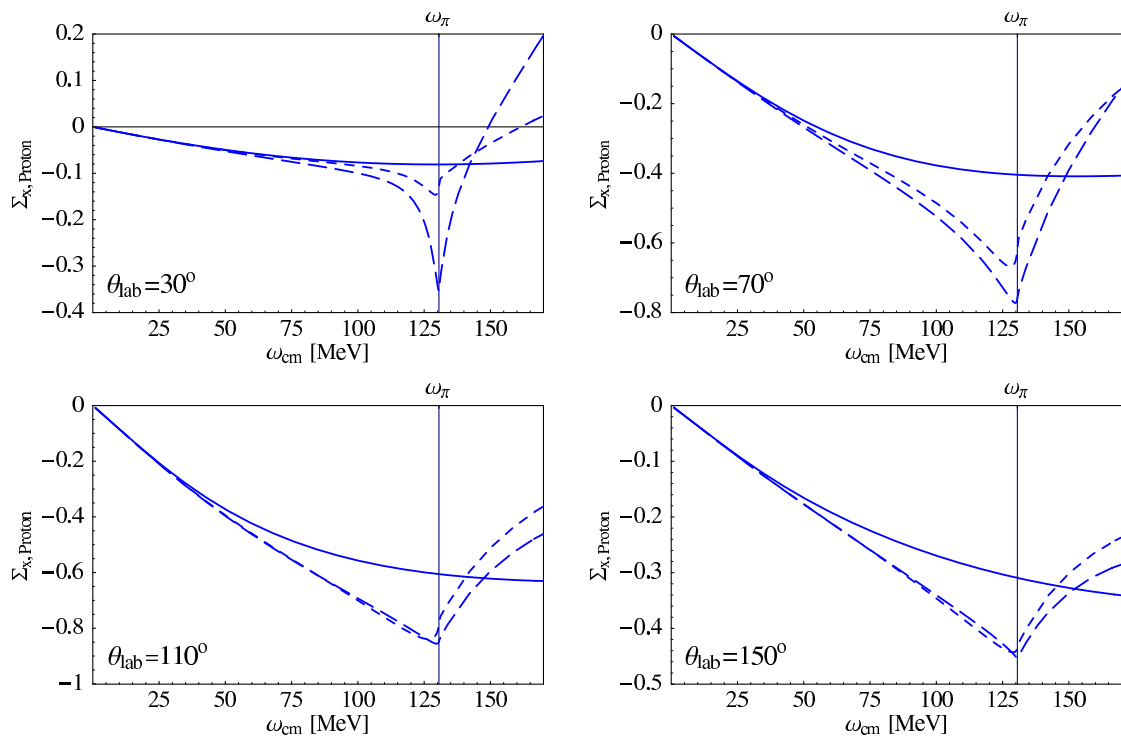


Fig. 6. Proton asymmetry Σ_x^p ; for notations see fig. 4.

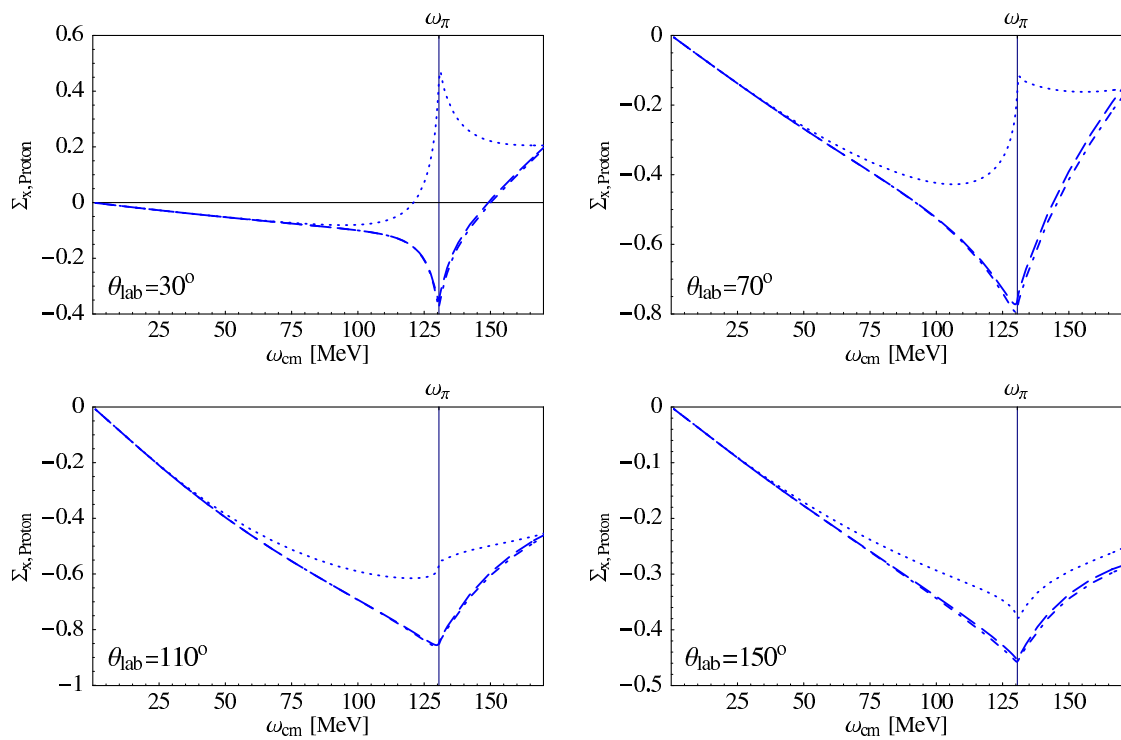


Fig. 7. Proton asymmetry Σ_x^p ; for notations see fig. 2.

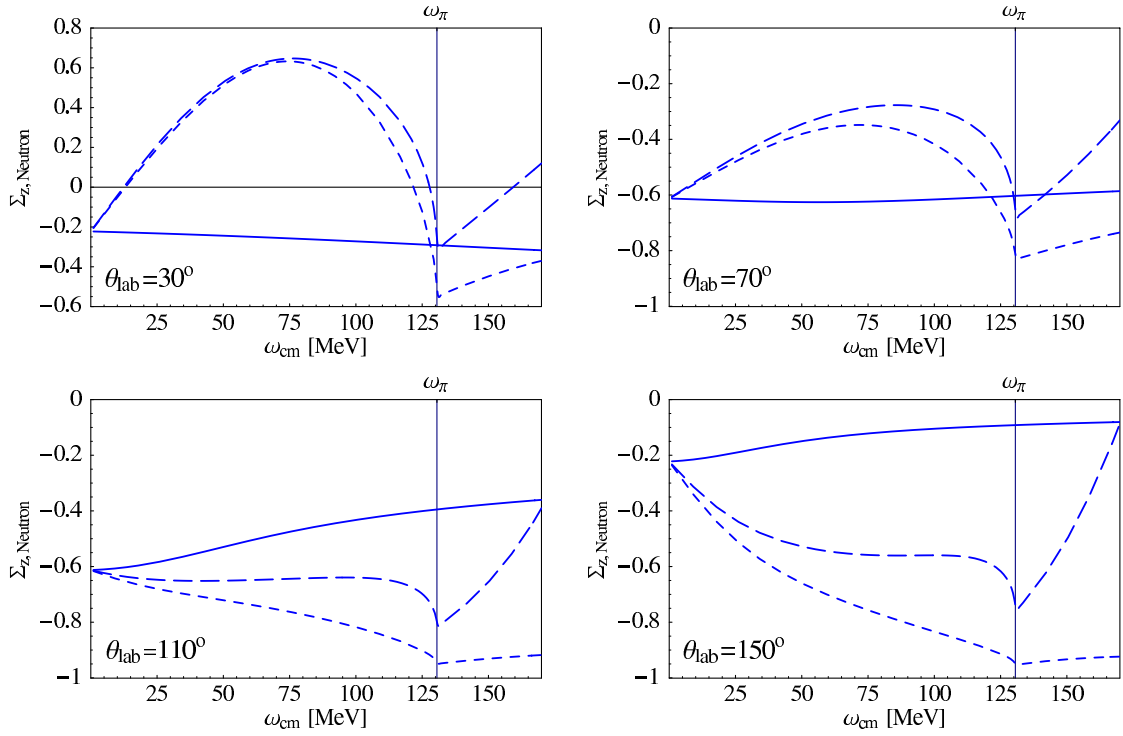


Fig. 8. Neutron asymmetry Σ_z^n ; for notations see fig. 4.

in sect. 6.1. Nonetheless, we find Σ_x^p more sensitive to the nucleon structure than Σ_z^p , especially around ω_π .

6.2.2 Spin and quadrupole contributions to Σ_x^p

As one can see in fig. 7, Σ_x^p is very sensitive to the spin polarizabilities for all angles. Therefore —and because of our findings in the previous subsection— this configuration (nucleon spin perpendicular to the photon momentum) seems to be more convenient than the spin parallel photon momentum, to examine the spin structure of the nucleon. In the backward direction, the spin dependence of the asymmetry is less pronounced than in the forward direction.

The quadrupole contributions are extremely small.

7 Neutron asymmetries

In the absence of stable single-neutron targets, the following results for the neutron have to be corrected for binding and meson exchange effects inside light nuclei, a task which will be the scope of future work. Here, we present the neutron results to guide considerations on future experiments using polarized deuterium or ^3He , *e.g.* [15].

As in the proton case, the neutron asymmetries reach quite large values of $\mathcal{O}(1)$ as the photon energy increases. In the neutron, pole contributions might be expected to be small, because it is uncharged and thus only the pion pole and anomalous magnetic moment contribute. On the

other hand, spin polarizabilities are then not enhanced by the interference with large pole amplitudes. Therefore, whether and which neutron asymmetries are sensitive to the structure parts, and hence to the γ_i 's, must be investigated carefully.

We follow the same line of presentation as outlined at the beginning of sect. 6 for the proton asymmetries: First, we investigate which internal degrees of freedom are seen in a specific asymmetry, and then show that quadrupole polarizabilities give negligible contributions. Thus, the asymmetries most sensitive to spin polarizabilities are identified.

7.1 Nucleon spin parallel photon momentum

7.1.1 Comparison: pole, HB χ PT and SSE calculation of Σ_z^n

Comparing fig. 8 to the proton analogs, figs. 4 and 6, we notice that the neutron is much more sensitive to the structure amplitudes. The pole curves show only a weak energy dependence, so that nearly the whole dynamics is given by the neutron polarizabilities. This minor influence of the pole amplitudes is due to the vanishing third-order pole contributions to A_1 and A_2 , which make the difference eq. (3.2) start with a term proportional to ω^2 , whereas the leading structure part is $\mathcal{O}(\omega^3)$. The spin-averaged cross-section starts with ω^2 , rendering the finite static values of Σ_z^n . The angular dependence of this static value can be derived from eqs. (2.3), (3.2), (3.4) as

$$\Sigma_z^n(\omega = 0, \theta) = \frac{4 \sin^2 \theta}{-5 + \cos(2\theta)}. \quad (7.1)$$

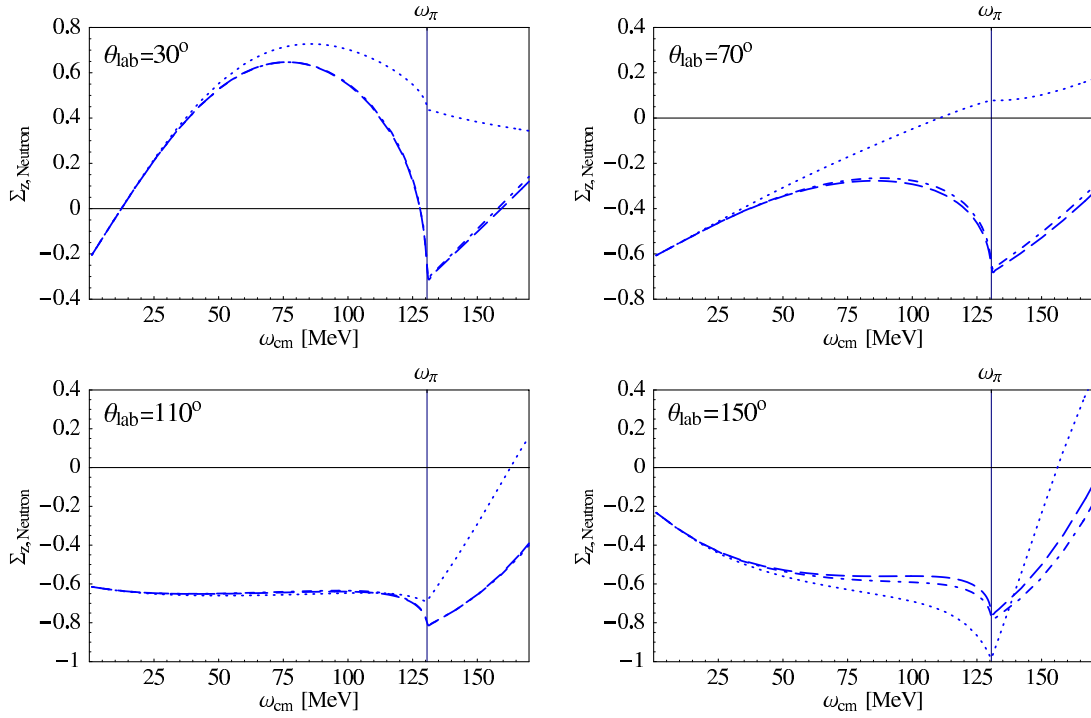


Fig. 9. Neutron asymmetry Σ_z^n ; for notations see fig. 2.

The structure sensitivity of the neutron is also visible in the huge sensitivity of Σ_z^n to the Δ -resonance which influences the polarized cross-sections considerably even for very low energies. As is well known, the influence of the $\Delta(1232)$ increases with increasing angle.

Concerning the shape of the asymmetry, one recognizes a similar behaviour for the whole angular spectrum. It always reaches a local minimum at the pion cusp. A precise interpretation of the shape of Σ_z^n is hard to give, as the denominator has the leading power ω^2 , while it was ω^0 in the proton case.

7.1.2 Spin and quadrupole contributions to Σ_z^n

Figure 9 shows that there are sizeable spin contributions to the asymmetry Σ_z^n for each angle, but for $\theta = 110^\circ$ they nearly completely vanish below the pion production threshold. The reason is the cancellation in the division of the difference by the sum. Nevertheless, one recognizes a decreasing spin dependence with increasing angle, which can again be explained by A_1 and A_3 . In the forward direction, A_3^{pole} starts with a falling slope and stays negative for the energy range we are considering. Adding the structure part of A_3 , *i.e.* including the spin polarizabilities, the amplitude changes sign roughly at the pion mass. Therefore we see a completely different behaviour of $A_1 \cdot A_3^{\text{pole}}$ and $A_1 \cdot A_3$ in the forward direction. In the backward direction A_1 , A_3 and A_3^{pole} are all positive below ω_π , resulting in very similar curves.

As in the proton case we find the quadrupole part to be negligibly small within the accuracy of this analysis (fig. 9).

7.2 Nucleon spin perpendicular to photon momentum

7.2.1 Comparison: pole, HB χ PT and SSE calculation of Σ_x^n

The shape of the asymmetry Σ_x^n in fig. 10 with the minimum at ω_π is similar to Σ_z^n (fig. 8), at least in the forward direction. The curve is shifted downward with increasing angle θ . An explanation for this behaviour can be given, though it is not obvious, as for $\theta \approx 0^\circ$, $\theta \approx 180^\circ$ there remain five terms in eq. (3.3): $[A_3 (A_3 - A_1) \cos \theta + A_3 A_4 (1 + \cos^2 \theta) + A_3 A_5 (3 \cos^2 \theta - 1) + 2 A_3 A_6 \cos \theta] \sin \theta \approx [A_3 (A_3 - A_1) \cos \theta + 2 A_3 (A_4 + A_5 + A_6 \cos \theta)] \sin \theta$. As can be read off eq. (2.3), the leading pole terms—which are linear in ω —vanish in the sum $A_4 + A_5 + A_6 \cos \theta$. Therefore, the lowest order in ω of $A_3 (A_4 + A_5 + A_6 \cos \theta)$ is ω^4 , since the spin-dependent structure amplitudes start with ω^3 . This is two orders in ω above the leading order of $A_3 (A_3 - A_1) \cos \theta$, which therefore is the leading term for small energies—at least for θ in the range from 30° to 150° . As can be read off appendix A, the product $A_1 A_3$ is negative for low energies in the forward direction, leading to a positive slope of the difference and therefore to positive values for the asymmetry. In the backward direction, $(A_3 - A_1)$, as well as A_3 , is positive, which gives a negative asymmetry as $\cos \theta < 0$. The angular dependence of the static value is

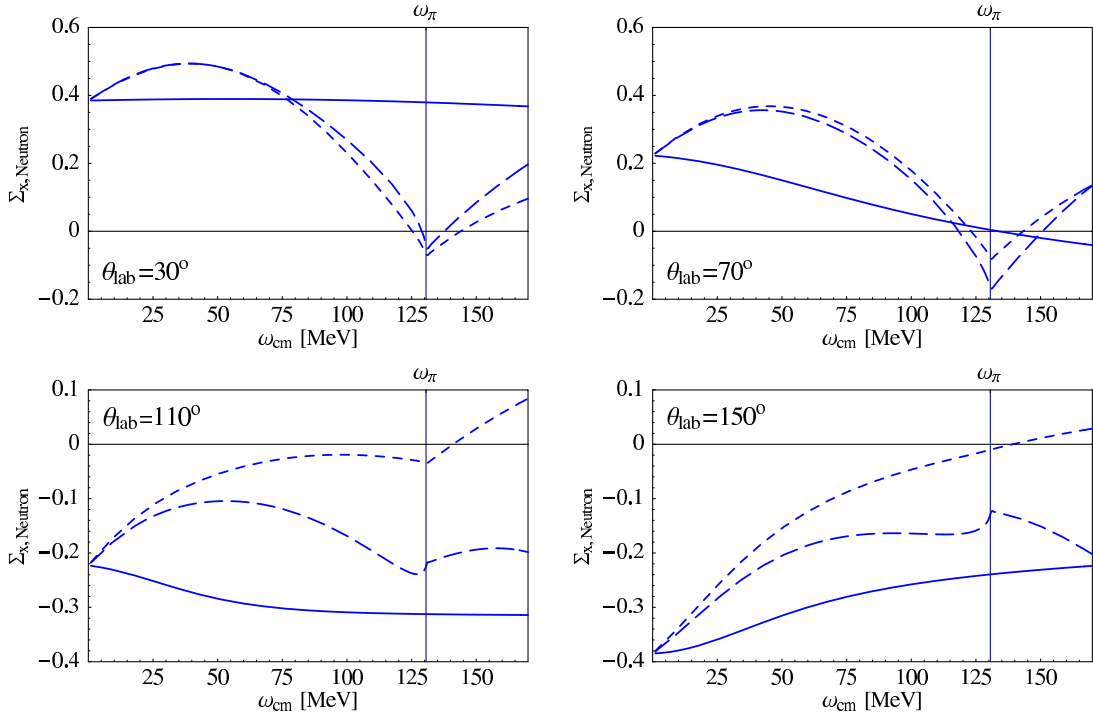


Fig. 10. Neutron asymmetry Σ_x^n ; for notations see fig. 4.

determined by the pole contributions. It is

$$\Sigma_x^n(\omega = 0, \theta) = \frac{4 \sin \theta \cos \theta}{5 - \cos(2\theta)}, \quad (7.2)$$

but as for Σ_z^n , the dynamics of Σ_x^n is completely dominated by the neutron polarizabilities.

Another interesting feature in fig. 10 is the fact, that the explicit Δ degrees of freedom only play a minor role in the forward direction but dominate for large angles.

7.2.2 Spin and quadrupole contributions to Σ_x^n

Turning to fig. 11, Σ_x^n exhibits of all asymmetries by far the largest sensitivity to the spin polarizabilities. Therefore, an experiment with the nucleon spin aligned perpendicular to the photon momentum seems from the theorist's point of view to be the most promising of the considered configurations to extract the spin polarizabilities. The weakest dependence on the γ_i 's at low energies of Σ_x^n occurs in the extreme forward direction. This again can be explained looking at A_1 and A_3 (fig. 12): In the backward direction, $A_3^{\text{pole}} < A_3$ and therefore also $(A_3^{\text{pole}} - A_1) < (A_3 - A_1)$, giving a much larger absolute value when spins are included. In the forward direction, A_3 differs weakly from A_3^{pole} for $\omega \leq 110$ MeV, so that spin polarizability effects appear only for higher energies.

As in Σ_z^n , the quadrupole polarizabilities in Σ_x^n are negligibly small (fig. 11). One observes the strongest contributions around $\theta = 90^\circ$; a simple answer to this phenomenon cannot be given, albeit it is clear that Σ_x^n should

be most sensitive at a scattering angle around 90° , as the overall factor $\sin \theta$ reaches its maximum (eq. (3.3)), but this is a general feature and not only concerning the quadrupole polarizabilities.

So as a short conclusion of sects. 6 and 7 we find a much stronger sensitivity of the neutron asymmetries to the nucleon structure, while the proton asymmetries are dominated by pole terms up to at least 50 MeV. Contributions of the $\Delta(1232)$ -resonance are crucial only for certain asymmetries and angles. For both nucleons, the spin configuration Σ_x turned out to be more sensitive to the nucleon spin structure than Σ_z . Dynamical quadrupole contributions are negligible in each of the considered cases.

8 Conclusion

In this work, we examined spin-averaged and double-polarized nucleon Compton cross-sections in the framework of Chiral Effective Field Theory as a guideline for future experiments. Our goal was to identify those experimental settings which are most likely to be sensitive to the four leading spin polarizabilities of the proton and neutron. These quantities parameterize the stiffness of the nucleon spin against electromagnetically induced deformations of definite multipolarity and non-zero frequency. Their energy dependence gives profound insight into the dispersive behaviour of the internal degrees of freedom of the nucleon, caused by internal relaxation effects, baryonic resonances and mesonic production thresholds, see also [12, 13] for details.

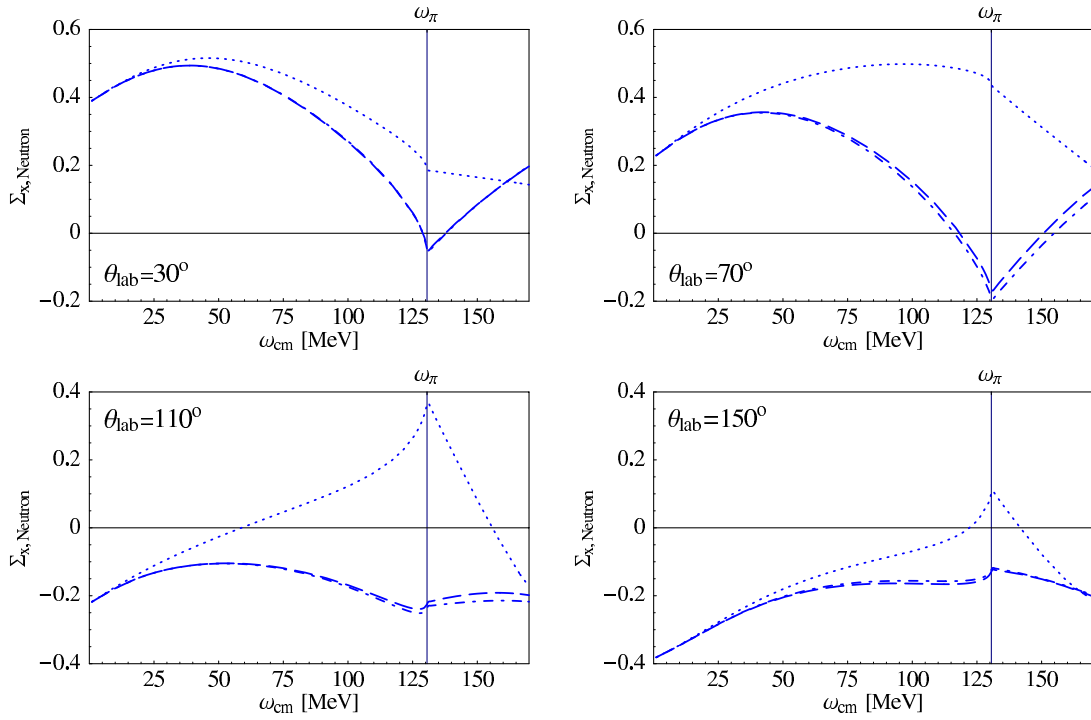


Fig. 11. Neutron asymmetry Σ_x^n ; for notations see fig. 2.

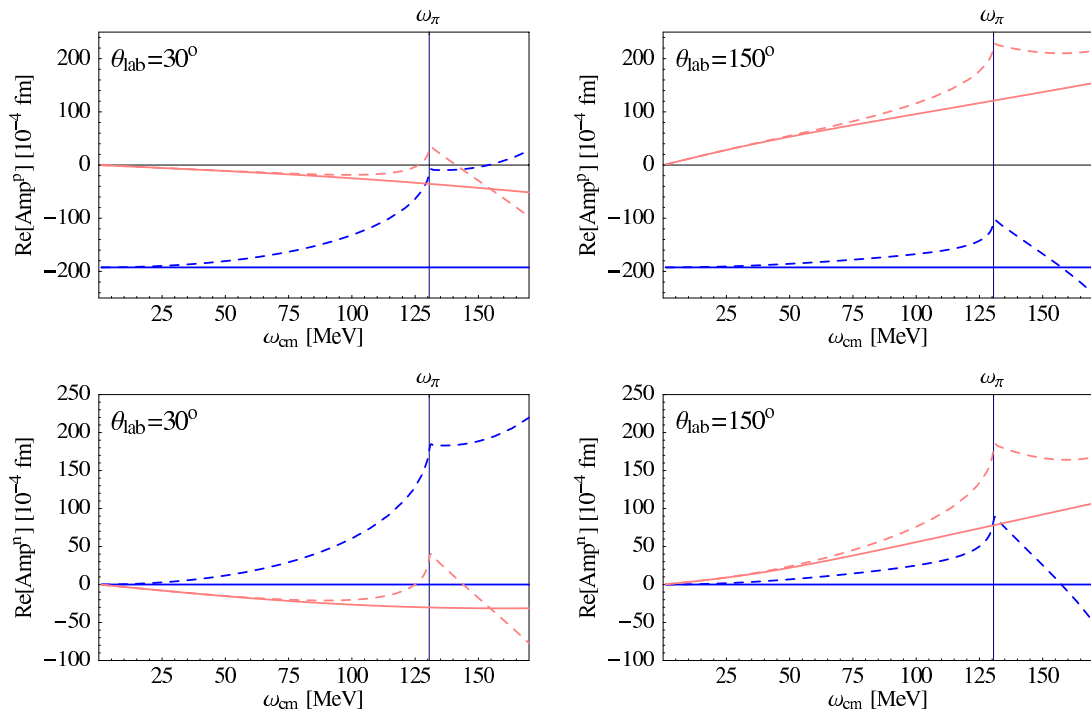


Fig. 12. $\mathcal{O}(\epsilon^3)$ SSE results for the real parts of the amplitudes A_1 (dark) and A_3 (light); the dashed line is the full $\mathcal{O}(\epsilon^3)$ SSE result, the solid line the third-order pole contribution, given in eq. (2.3); the upper (lower) panels show the proton (neutron) results. Recall that for the neutron, $A_1^{\text{pole}} = 0$.

In the spin-averaged cross-sections, sect. 5, we found significant deviations between predictions with and without spin polarizabilities. Therefore, spin-averaged experiments can contribute to a direct determination of *dynamical spin* polarizabilities from data, too.

In the polarized case, sects. 6 and 7, we considered configurations with a right-circularly polarized incident photon and a polarized target nucleon, leaving the spins of the particles in the final state undetected. We investigated the dependence of the cross-sections and asymmetries on the spin polarizabilities in two different spin configurations: i) nucleon spin parallel minus antiparallel to the photon momentum, and ii) perpendicular to it but still inside the reaction plane. We noted a stronger sensitivity in the asymmetry Σ_x of configuration ii) for both proton and neutron targets, than in case i). We found furthermore that only two of the structure amplitudes, namely A_1 and A_3 , dominate all cross-sections and asymmetries.

The spin polarizabilities give usually the clearest signal for photon energies above 100 MeV, say around the pion production threshold (~ 130 MeV), where most of the asymmetries also reach $\mathcal{O}(1)$. In the backward direction, the neutron asymmetries also show a strong sensitivity to the physics of the $\Delta(1232)$ -resonance, in addition to contributions from the chiral pion cloud around the nucleon.

In general, the neutron asymmetries were found to be more sensitive to the spin polarizabilities than the proton analogs. This is no surprise, since Compton scattering on the charged proton is dominated by the pole amplitudes. Besides the resulting minor sensitivity to the nucleon structure, another disadvantage of the proton asymmetries is the small spin-averaged cross-section around the pion production threshold for small angles, which enhances theoretical uncertainties. Again, we emphasize that up to leading-one-loop order the only difference between proton and neutron is given by the pole contributions, *i.e.* the structure part of our amplitudes is the one of an isoscalar nucleon. Polarized cross-sections, which are calculated in this approximation, might therefore deviate from experimental results, especially for the neutron, where the pole contributions are weak. Hints on important isovector contributions are given in [22], where the non-pion-pole contribution to the backward spin polarizability γ_π of the neutron was found to be about twice as large as the corresponding proton value.

Contributions of the quadrupole polarizabilities turned out to be negligibly small, as in the spin-averaged case [13]. Therefore, like spin-averaged observables, spin-polarized cross-sections are well described by only six energy-dependent functions: the two spin-independent and four spin dipole polarizabilities. This led us in sect. 4 to propose to extract the energy dependence of the four spin polarizabilities of the individual nucleons by a model-independent multipole expansion of the structure amplitudes from a combination of polarized and unpolarized precision experiments. Chiral Effective Field Theory with explicit $\Delta(1232)$ degrees of freedom represents correctly the symmetries and low-energy degrees of freedom inside the nucleon in a model-independent way. One can there-

fore in a first step accept our predictions of the energy dependence of the polarizabilities as induced by dispersive effects and only fit their overall normalization to experiment, thus obtaining their static values. At present, only two linear combinations, γ_0 and γ_π , were measured experimentally on the proton at LEGS [6] and MAMI [7, 8], with partially conflicting values.

Clearly, the lack of free-neutron targets makes an extension of the work presented here to light nuclei mandatory if experiments are to be interpreted, especially in the light of feasibility studies on Compton scattering on the deuteron and ^3He at HI γ S/TUNL [15]. Work is therefore under way to consider spin-polarized observables on these configurations [16], utilizing the chiral potential approach [23] and extending already existing calculations on unpolarized Compton scattering off light nuclei in Chiral Effective Field Theories [24]. Further investigations involving linearly polarized photon beams are also in preparation [16]. We are therefore confident that such future experiments will further our understanding of a fundamental property of the nucleon: the response of its effective low-energy degrees of freedom, and in particular of its spin, in electric and magnetic fields, as parameterized in the dipole polarizabilities.

The authors acknowledge helpful discussions with H. Gao and W. Weise. We are grateful to the ECT* in Trento for its hospitality. This work was supported in part by the Bundesministerium für Forschung und Technologie, and by Deutsche Forschungsgemeinschaft under contract GR1887/2-1 (H.W.G. and R.P.H.).

Appendix A. Dominant amplitudes at low energies

In fig. 12, we plot A_1 and A_3 at forward and backward angles, as we found in sects. 5, 6 and 7 many low-energy features in our results for polarized and unpolarized cross-sections that can be explained by considering only these two amplitudes. The amplitudes of the uncharged neutron vanish for $\omega = 0$ while the static value of A_1^p is given by the Thomson limit. The clear cusp structure arises from $\alpha_{E1}(\omega)$ in A_1 and from $\gamma_{E1E1}(\omega)$ in A_3 , cf. eq. (2.2) and [13].

References

1. D. Drechsel, B. Pasquini, M. Vanderhaeghen, Phys. Rep. **378**, 99 (2003).
2. B.R. Holstein *Chiral perturbation theory and nucleon polarizabilities*, in *Chiral Dynamics 1997: Theory and Experiment*, edited by A.M. Bernstein, D. Drechsel, T. Walcher (Springer-Verlag, Berlin, 1998), hep-ph/9710548.
3. T.R. Hemmert, *Nucleon Compton scattering in chiral effective field theories*, in *Chiral Dynamics 2000: Theory and Experiment*, edited by A.M. Bernstein, J. Goity, U.-G. Meißner (World Scientific, Singapore, 2001), nucl-th/0101054.
4. S. Ragusa, Phys. Rev. D **47**, 3757 (1993).

5. GDH Collaboration (J. Ahrens *et al.*), Phys. Rev. Lett. **87**, 022003 (2001).
6. J. Tonnison, A.M. Sandorfi, S. Hoblit, A.M. Nathan, Phys. Rev. Lett. **80**, 4382 (1998).
7. V. Olmos de Leon *et al.*, Eur. Phys. J. A **10**, 207 (2001).
8. G. Galler *et al.*, Phys. Lett. B **503**, 245 (2001).
9. S. Wolf *et al.*, Eur. Phys. J. A **12**, 231 (2001).
10. M. Camen *et al.*, Phys. Rev. C **65**, 032202(R) (2002).
11. T.R. Hemmert, B.R. Holstein, J. Kambor, G. Knöchlein, Phys. Rev. D **57**, 5746 (1998).
12. H.W. Griesshammer, T.R. Hemmert, Phys. Rev. C **65**, 045207 (2002).
13. R.P. Hildebrandt, H.W. Griesshammer, T.R. Hemmert, B. Pasquini, this issue, p. 293, nucl-th/0307070.
14. D. Babusci, G. Giordano, A.I. L'vov, G. Matone, A.M. Nathan, Phys. Rev. C **58**, 1013 (1998).
15. H. Gao, private communication (2002, 2003).
16. R.P. Hildebrandt, H.W. Griesshammer, T.R. Hemmert, D.R. Phillips, in preparation; R.P. Hildebrandt *et al.*, in preparation.
17. V. Bernard, N. Kaiser, U.-G. Meißner, Int. J. Mod. Phys. E **4**, 193 (1995).
18. T.R. Hemmert, B.R. Holstein, J. Kambor, J. Phys. G **24**, 1831 (1998).
19. Particle Data Group, *Review of Particle Physics*, Phys. Rev. D **66**, 010001 (2002).
20. V. Bernard, N. Kaiser, J. Kambor, U.-G. Meißner, Nucl. Phys. B **388**, 315 (1992).
21. T.R. Hemmert, B.R. Holstein, J. Kambor, Phys. Rev. D **55**, 5598 (1997).
22. K. Kossert *et al.*, Eur. Phys. J. A **16**, 259 (2003).
23. See, *e.g.*, E. Epelbaum, A. Nogga, W. Glöckle, H. Kamada, U.-G. Meißner, H. Witala, Eur. Phys. J. A **15**, 543 (2002) and references therein.
24. *E.g.*, S.R. Beane, M. Malheiro, D.R. Phillips, U. van Kolck, Nucl. Phys. A **656**, 367 (1999); S.R. Beane, M. Malheiro, J.A. McGovern, D.R. Phillips, U. van Kolck, Phys. Lett. B **567**, 200 (2003).